Superexcited states of oxygen studied by fast-electron impact

Lan-Lan Fan,[1] Zhi-Ping Zhong,[2,*] Lin-Fan Zhu,[1] Xiao-Jing Liu,[1] Zhen-Sheng Yuan,[1] Jian-Min Sun,[1] and Ke-Zun Xu[1]
[1]*Hefei National Laboratory for Physical Sciences at Microscale, Department of Modern Physics, University of Science and Technology of China, Hefei, Anhui, 230026, China*
[2]*College of Physical Science, Graduate School of the Chinese Academy of Sciences, P.O. Box 4588, Beijing 100049, China*
(Received 23 August 2004; published 8 March 2005)

Absolute double differential cross section spectra of O_2 at scattering angles of 0°, 2°, 4°, 6°, and 8° below 119 eV have been determined by the angle-resolved electron-energy-loss spectrometer at an incident electron energy of 2500 eV. Some features above the first ionization threshold stand out as the momentum transfer square K^2 increases. Based on our experimental results and theoretical analysis, they are assigned to the optically forbidden Rydberg series of $2\sigma_u^{-1}(c\,^4\Sigma_u^-)np\sigma_u\,^3\Sigma_g^-$ ($n=2$–6) and the inner-valence transition of $(2\sigma_g)^{-1}(1\pi_g)^3\,^3\Pi_g \leftarrow X\,^3\Sigma_g^-$, respectively. Furthermore, the observed energy positions of $2\sigma_u^{-1}(c\,^4\Sigma_u^-)np\sigma_u\,^3\Sigma_g^-$ ($n=2$–6) confirm a theoretical prediction [Zhong and Li, J. Phys. B **37**, 735 (2004)] that the eigenquantum defects show an evident oscillation due to the presence of shape resonance.

DOI: 10.1103/PhysRevA.71.032704 PACS number(s): 34.80.Gs, 33.70.Fd, 31.15.Ne

I. INTRODUCTION

The definition, nature, use, and supposed miraculous capabilities of shape resonance have been discussed intensively for more than one decade [1]. Theoretically, Dehmer and Dill [2] predicted that f-wave enhancement in the σ (σ_u for homonuclear diatomic molecules) channel would result in the enhancement of the photoionization cross section. Recently, Zhong and Li [3] calculated the eigenquantum defects μ ($\mu=\tau/\pi$, where τ is the short-range phase shift above threshold) of the CO molecule. Their results indicate that different partial waves mix with each other strongly and no partial wave is dominant in each eigenchannel close to the energy position of a shape resonance. Such calculations agree with the ion-electron coincidence measurements of fixed-in-space molecules [4,5], in which it is indicated that several partial waves, at least $l=1$, 2, and 3, give comparable contributions to the shape resonances. Furthermore, based on the calculations of Zhong and Li [3], μ's in the σ channel evidently oscillate around the energy position of a shape resonance. Such oscillation cannot be observed in the experimental spectrum unless the shape resonance is embedded in a Rydberg series in the σ channel, i.e., the shape resonance occurs below the threshold. Up to now, this type of oscillation has not been observed.

Molecular oxygen, whose ground state can be written as $KK(2\sigma_g)^2(2\sigma_u)^2(3\sigma_g)^2(1\pi_u)^4(1\pi_g)^2$, may be a good candidate for observing such oscillation, since the O 1s shape resonance occurs below the threshold [6]. However, it is difficult to verify this oscillation in the O K-shell spectrum, because the high n Rydberg structures in the O K-shell spectrum are veiled due to insufficient energy resolution or poor signal-to-noise ratios. Such oscillation cannot be observed either in the optically allowed shape resonances in the energy region of valence excitation which is related to the excitation of a $1\pi_g$ or $3\sigma_g$ electron. More specifically, the shape resonance related to the excitation of a $1\pi_g$ electron occurs near the threshold at about 12 eV [7]. However, no experimental data have been reported about $np\sigma_u \leftarrow 1\pi_g$ transitions due to the small intensity and overlapping with many autoionization states. There is only one shape resonance at 22.6 eV above threshold in the photoionization to the $3\sigma_g^{-1}$ channels instead of two separated multiplet-specific shape resonances, because a significant interchannel coupling effect exists in these channels [7]. It is an interesting question whether such oscillation can be observed in the optically forbidden Rydberg series related to the excitation of a $2\sigma_u$ electron. This question may be answered by angle-resolved electron-energy-loss spectroscopy (AREELS), which is a powerful tool for investigating the structures of atomic and molecular energy levels including both the optically allowed and optically forbidden transitions. In addition, the recent experimental work on NO [8] and calculation on CO [9] elucidate that AREELS is an important method to investigate the structures of superexcited states, i.e., excited states of molecules above the first ionization threshold such as high Rydberg states, doubly or inner-shell excited, non-Rydberg states, etc. [10–12]. Since the momentum transfer dependence behaviors of different superexcited states are different, some superexcited states may stand out at large scattering angles.

In this work, we have measured the electron-energy-loss spectra of O_2 in the scattering angle range of 0°–8° with an interval of 2°, and the absolute optical oscillator strength density (OOSD) and double differential cross section (DDCS) have been determined. Some features above the first ionization threshold stand out at large scattering angles. Combining with the present theoretical analysis, these features are assigned. Furthermore, evident oscillation of the eigenquantum defects due to the presence of shape resonance is observed.

II. EXPERIMENTAL AND THEORETICAL METHOD

The angle-resolved electron-energy-loss spectrometer used in this work has been described in detail in Refs.

*Corresponding author. Email address: zpzhong@gscas.ac.cn

[13–15]. Briefly, it consists of an electron gun, a hemispherical electrostatic monochromator made of aluminium, a rotatable energy analyzer of the same type, an interaction chamber, a number of cylindrical electrostatic lenses, and a one-dimension position-sensitive detector for detecting the scattered electrons. All of these components are enclosed in four separate vacuum chambers made of stainless steel. The impact energy of the spectrometer can be varied from 1 to 5 keV. For the present experiment, it was set at 2.5 keV and the energy resolution was about 100 meV. All the spectra were measured at the pressure of 8×10^{-3} Pa and the background pressure in the vacuum chamber was 5×10^{-5} Pa. The true zero angle was calibrated by the symmetry of the angular distribution of the $E\,^3\Sigma_u^-,\ \nu'=0\leftarrow X\,^3\Sigma_g^-$ inelastic scattering signal around the geometry nominal zero. The angular resolution was about 0.8° at present.

The electron-energy-loss spectra of O_2 were measured in the scattering angle range of 0°–8° with an interval of 2°, and calibrated at 9.970 eV according to the transition of $E\,^3\Sigma_u^-,\ \nu'=0$ [16]. Then, the spectrum measured at a mean scattering angle of 0° was converted into relative OOSD spectrum by multiplying the Bethe-Born conversion factor of the spectrometer [13,17]. The spectra at the other scattering angles were converted into relative generalized oscillator strength density (GOSD) spectra according to the following Bethe-Born formula [18,19] within the nonrelativistic Born approximation:

$$\frac{df(E,K)}{dE}=\frac{E}{2}\frac{p_0}{p_a}K^2\frac{d^2\sigma}{dEd\Omega}. \tag{1}$$

Here, $df(E,K)/dE$ and $d^2\sigma/(dEd\Omega)$ represent GOSD and DDCS, E and K are the excitation energy and momentum transfer while p_0 and p_a are the incident and scattered electron momenta, respectively.

These relative GOSD spectra were made absolute by the valence shell Bethe sum rule [18,20]:

$$S_{val}(0)=N_{val}+N_{PE}=\int_{E'}^{\infty}\left(\frac{df}{dE}\right)dE, \tag{2}$$

where N_{val} is the total number of valence electrons in the target (12 for O_2), N_{PE} is a small correction (0.42 for O_2) for the Pauli-excluded transitions from the K shell to the already occupied valence shell orbitals [21,22], and E' is the lowest excitation energy. In the limit of $K\to0$, the GOSD is identical to the OOSD which was obtained using the valence Thomas-Reiche-Kuhn (VTRK) sum rule [23]. In the sum-rule normalization procedure, the intensity of the relative OOSD or GOSD obtained at a definite scattering angle was first numerically integrated over a sampling energy-loss range, i.e., up to 81 eV for 0°, 119 eV for 2°, 4°, 6°, and 8°. The remaining intensity of the valence shell higher than the measured energy region for O_2 was estimated by integrating a fitted function $aE^{-1.5}+bE^{-2.5}+cE^{-3.5}$ from the limit energy of the measurements to infinity, where the empirical parameters a, b, and c were obtained by least-squares fitting a smoothly decreasing region, i.e., 50–81 eV for 0°, 50–119 eV for 2°, 60–119 eV for 4°, 80–119 eV for 6° and 8°, respectively. The overall percent error of the OOSD and DDCS obtained in this work is about 20%, which mainly comes from the instability of beam current, the angle determination, the angular correction factor, the statistics of counts, and the least-squares fitting procedure.

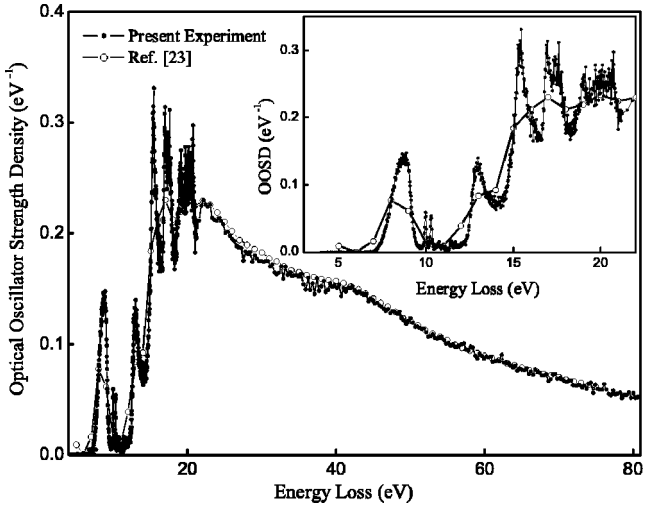

FIG. 1. Absolute OOSD of O_2 in the energy region of 4–81 eV. The inset figure exhibits the expanded spectra in the energy region of 4–22 eV.

The multiscattering self-consistent-field (MSSCF or MS-X_α) method was employed in this work. Briefly, based on a trial charge density of the molecule, a muffin-tin trial molecular potential V^{mol} with the symmetry of molecular point group was constructed. We can then calculate the occupied molecular orbitals (MOs), which serve to construct the charge density of the molecule and then a new trial molecular potential. With this process going on, self-consistent iterations were undertaken until a certain precision was met. A self-consistent-field (SCF) molecular potential V_{scf}^{mol} was obtained and thereafter we can calculate all the MOs, including nondiffusive molecular orbitals (NMOs), Rydberg molecular orbitals (RMOs), and adjacent continuum molecular orbitals (CMOs), respectively. In our calculations, all the RMOs and CMOs were treated in a unified manner in the framework of quantum defect theory (QDT) [24–28]. With the calculated wave functions, the GOSD can be calculated as follows [18]:

$$\frac{df(K,E)}{dE}=\sum_n\frac{E_n}{K^2}|\langle\Psi_n|\sum_{j=1}^{N}\exp(i\mathbf{K}\cdot\mathbf{r}_j)|\Psi_0\rangle|^2\delta(E_n-E).$$

Here, Ψ_0 and Ψ_n are the electronic wave functions of the initial and the final states, respectively, N is the anticipated number of electrons in the target particle, E_n is the excitation energy, and $\mathbf{r}_j$ is the position of the jth electron.

III. RESULTS AND DISCUSSION

The present absolute OOSD is shown in Fig. 1 together with the one determined by the same method as ours but with a higher impact energy of 8 keV and a lower energy resolution of 1 eV [23]. Clearly, the spectra are in good agreement with each other above 22 eV. The expanded spectra below 22 eV are shown in the inset graph in Fig. 1. The discrepancy

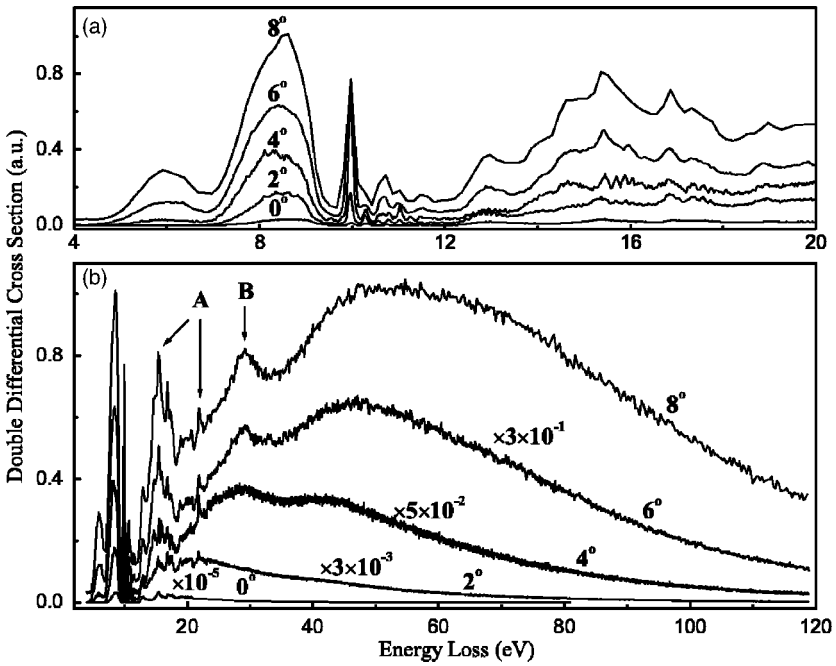

FIG. 2. DDCSs measured at 0°, 2°, 4°, 6°, and 8° (a) in the energy region of 4–20 eV; (b) in the energy region of 4–120 eV.

can be attributed to the different energy resolution.

In Fig. 2, we present the absolute DDCS spectra below 120 eV at scattering angles of 0°, 2°, 4°, 6°, and 8°. It can be seen clearly that the energy position of the very broad features observed at 6° and 8°, i.e., the Bethe ridge, moves to higher energy loss and becomes more diffuse with the increase of K^2. Such phenomena have also been observed in other molecules such as NO [8], H_2O [29], and SF_6 [30]. Furthermore, some features marked as *A* and *B* stand out as K^2 increases. These features will be discussed in detail in the order of excitation energy.

The spectra of O_2 in the energy region of 12–25 eV are shown in Fig. 3 with the experimental ionization thresholds [31,32] for valence-hole states. The assignments in Fig. 3(a) are cited from Refs. [33–37] except that the energy positions of the vibrational levels of $1\pi_u^{-1}(A\,^2\Pi_u)4s\sigma_g$ are calculated using the molecular constants of $1\pi_u^{-1}(A\,^2\Pi_u)3s\sigma_g$ [36] since they belong to the same Rydberg series. The Rydberg states denoted by *I*, *I′*, and *I″* are three bound electronic states converging to the $a\,^4\Pi_u$ state of O_2^+ [35]. Here *R*(*A*) in Fig. 3(a) represents the Rydberg series converging to ionization

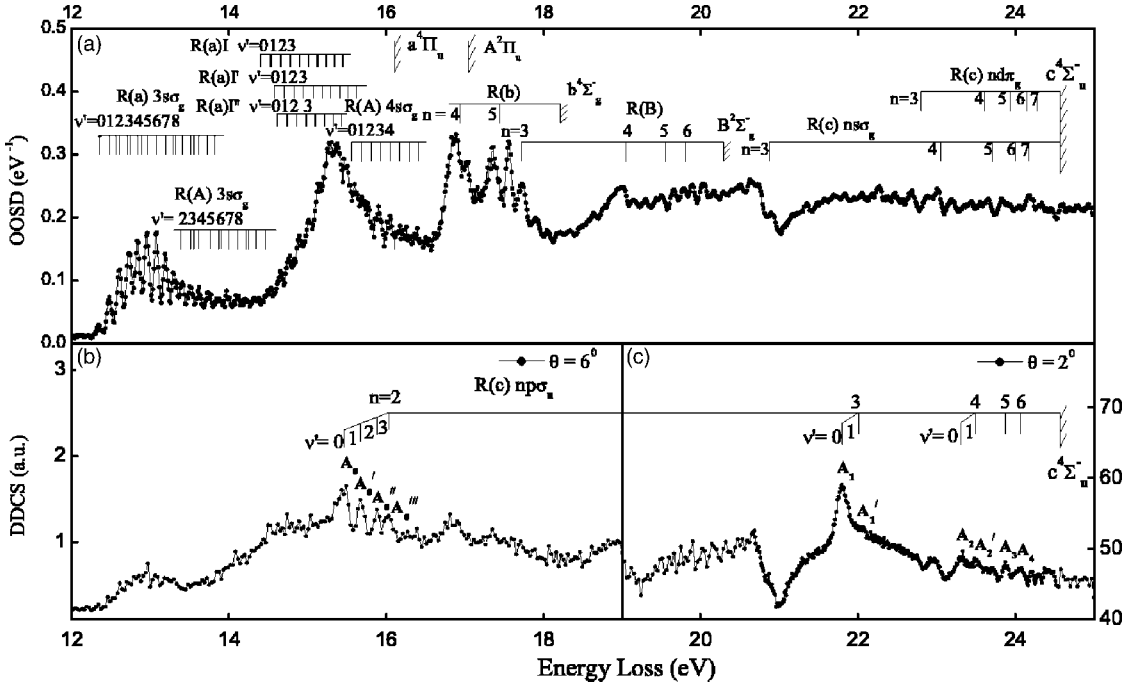

FIG. 3. The spectra and assignments of O_2 in the energy region of 12–25 eV (a) OOSD; (b) DDCS measured at 6°; (c) DDCS measured at 2°.

TABLE I. The excitation energies, effective numbers $n^{\star}$, and quantum defects μ of observed $(2\sigma_u)^{-1}(c\,^4\Sigma_u^-)np\sigma_u$ ($n=2$–6) series in molecular oxygen.

	Energy (eV)			$n^{\star}$			μ			
Feature	Present (± 0.02)	Ref. [39]	Ref. [39][a]	Present	Ref. [39]	Ref. [39][a]	Present	Ref. [39]	Ref. [39][a]	Assignment
A_0	15.46			1.22			0.78			$(2\sigma_u)^{-1}(c\,^4\Sigma_u^-)2p\sigma_u v'=0$
A_0'	15.67									$(2\sigma_u)^{-1}(c\,^4\Sigma_u^-)2p\sigma_u v'=1$
A_0''	15.88									$(2\sigma_u)^{-1}(c\,^4\Sigma_u^-)2p\sigma_u v'=2$
A_0'''	16.03									$(2\sigma_u)^{-1}(c\,^4\Sigma_u^-)2p\sigma_u v'=3$
A_1	21.80	21.85	21.82	2.22	2.24	2.23	0.78	0.76	0.77	$(2\sigma_u)^{-1}(c\,^4\Sigma_u^-)3p\sigma_u v'=0$
A_1'	22.01									$(2\sigma_u)^{-1}(c\,^4\Sigma_u^-)3p\sigma_u v'=1$
A_2	23.31	23.30	23.31	3.29	3.28	3.29	0.71	0.72	0.71	$(2\sigma_u)^{-1}(c\,^4\Sigma_u^-)4p\sigma_u v'=0$
A_2'	23.49									$(2\sigma_u)^{-1}(c\,^4\Sigma_u^-)4p\sigma_u v'=1$
A_3	23.87	23.80	23.87	4.43	4.22	4.43	0.57	0.78	0.57	$(2\sigma_u)^{-1}(c\,^4\Sigma_u^-)5p\sigma_u v'=0$
A_4	24.06	24.06	24.06	5.20	5.20	5.20	0.80	0.80	0.80	$(2\sigma_u)^{-1}(c\,^4\Sigma_u^-)6p\sigma_u v'=0$

[a]Obtained by digitizing the Fig. 3 in Ref. [39].

threshold $A\,^2\Pi_u$, the rest in Fig. 3(a) and those in Fig. 3(b) are similar.

The feature marked as A in Fig. 2 consists of A_0, A_0', A_0'', A_0''', A_1, A_1', A_2, A_2', A_3, and A_4 as shown in Figs. 3(b) and 3(c), their energy positions are listed in Table I. Note that A_0, A_0', A_0'', and A_0''', which have not been observed before, are almost equidistant with an energy interval of about 0.2 eV. They may be a vibrational progression of an electronic state. Such electronic state should not correspond to the excitation of a bonding orbital electron (e.g., $1\pi_u$ or $3\sigma_g$) since vibrational energy intervals related to the excitation of a bonding orbital electron are much smaller than 0.2 eV. Therefore this electronic state may be related to the excitation of an antibonding orbital electron $2\sigma_u$. Similarly, the energy interval between A_1 and A_1' is almost equal to 0.2 eV. They may be a vibrational progression of an electronic state, and this electronic state may also be related to the excitation of an antibonding orbital electron $2\sigma_u$. It is the same situation for A_2 and A_2'. As shown in Table I, the quantum defects of A_0, A_1, A_2, A_3, and A_4 are almost constant except that of A_3 when the ionization threshold is taken as that of $2\sigma_u^{-1}(c\,^4\Sigma_u^-)$ (24.564 eV) [31]. Meanwhile, the intensity behavior among A_1, A_2, A_3, and A_4, which decreases as excitation energy increases, is similar to the behavior of a Rydberg series. Therefore we assign features A_0, A_1, A_2, A_3, and A_4 to the Rydberg series of $2\sigma_u^{-1}(c\,^4\Sigma_u^-)np\sigma_u\,^3\Sigma_g^-$, $v'=0$ ($n=2$–6, $2p\sigma_u$ corresponds to the unoccupied orbital $3\sigma_u$), and A_0, A_1, and A_2 have several vibrational components as shown in Figs. 3(b) and 3(c).

Now, we discuss the reason why the quantum defect of A_3 evidently deviates from those of A_0, A_1, A_2, and A_4. Figure 4 shows our calculated quantum defects in the σ_u channel with the present experimental ones of A_1, A_2, A_3, and A_4. Clearly, the present experimental quantum defects are close to the calculated ones in the $p\sigma_u$ channel. Moreover, the well-known σ_u resonance is also demonstrated in our calculations, i.e., there is a rapid increase of the eigenquantum defect by 1 near threshold in the $f\sigma_u$ channel. Our calculations show that the presence of this shape resonance results in the oscillation of quantum defects in the $p\sigma_u$ channel. Therefore it is understandable that the quantum defect of A_3 evidently deviates from those of A_0, A_1, A_2, and A_4. The different energy positions of such oscillation between experimental and calculated data may be due to the neglecting of electronic correlation (i.e., channel interactions) in the present calculations. In addition, comparing with only the $v'=0$ and 1 levels supported by the optically allowed Rydberg series converging to $c\,^4\Sigma_u^-$ [33], $2\sigma_u^{-1}(c\,^4\Sigma_u^-)2p\sigma_u$ shows unusual vibrational structures, i.e., more than two vibrational levels. Such phenomenon is similar to that in the K-shell spectrum of O_2, which is due to the fact that the $3p\sigma \leftarrow 1s$ Rydberg excited state is strongly perturbed by the repulsive state of $2p\sigma_u \leftarrow 1s$ [38]. Therefore it is suggested that the strong interaction between $3p\sigma_u \leftarrow 2\sigma_u$ Rydberg excited state and $2p\sigma_u \leftarrow 2\sigma_u$ valence state results in the unusual vibrational structures of $2\sigma_u^{-1}(c\,^4\Sigma_u^-)2p\sigma_u$.

Dillon and Spence [39] have also observed the same optically forbidden Rydberg series $2\sigma_u^{-1}(c\,^4\Sigma_u^-)np\sigma_u\,^3\Sigma_g^-$ (n

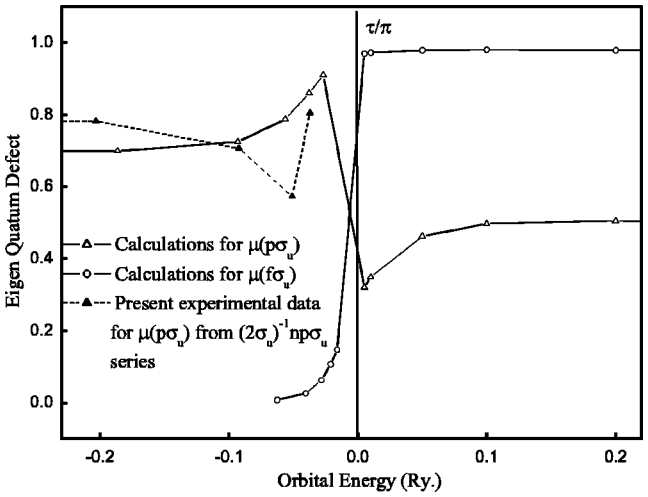

FIG. 4. The calculated and experimental quantum defects in the σ_u channel.

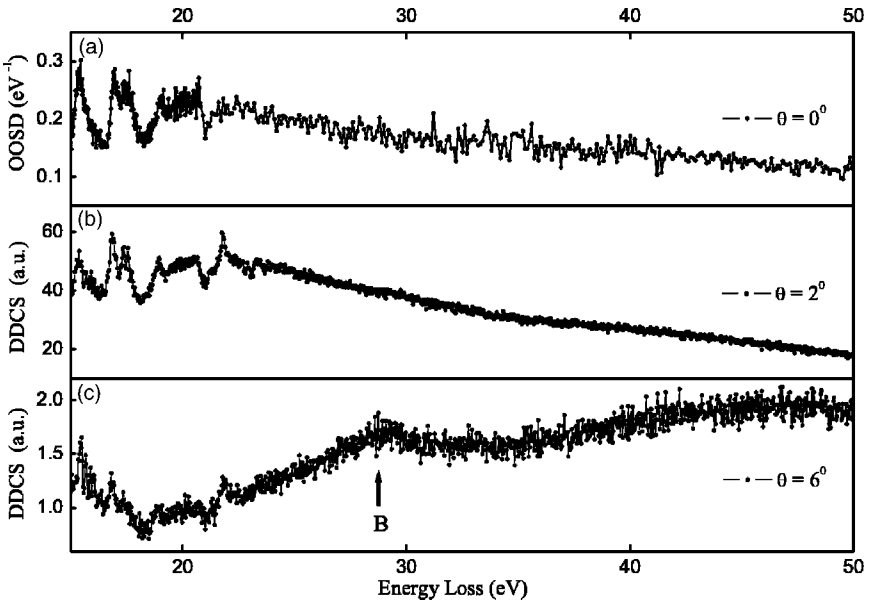

FIG. 5. The spectra of O_2 in the energy region of 15–50 eV (a) OOSD; (b) DDCS measured at 2°; (c) DDCS measured at 6°.

=3–6) with a similar experimental method. Their observed energy positions of $2\sigma_u^{-1}(c\,^4\Sigma_u^-)np\sigma_u$ (n=3–6) are also listed in Table I. Note that there are evident discrepancies for $2\sigma_u^{-1}(c\,^4\Sigma_u^-)3p\sigma_u$ and $2\sigma_u^{-1}(c\,^4\Sigma_u^-)5p\sigma_u$ between ours and that of Dillon and Spence [39]. The present count for each energy point in the energy region covering $2\sigma_u^{-1}(c\,^4\Sigma_u^-)np\sigma_u$ (n=3–6) Rydberg series is more than 2.5×10^4 and the measured energy interval is 0.01 eV. Therefore the discrepancy cannot be attributed to statistic errors. After digitizing the spectrum shown as Fig. 3 in Ref. [39], the energy positions of $2\sigma_u^{-1}(c\,^4\Sigma_u^-)np\sigma_u$ (n=3–6) were obtained as shown in Table I. It is found that the digitized results agree well with ours. Therefore our energy positions of $2\sigma_u^{-1}(c\,^4\Sigma_u^-)np\sigma_u$ (n=2–6) are recommended.

As shown in Fig. 5, a broad feature around 28.8 eV marked as B in Fig. 2 is not clearly observed until the scattering angle reaches 6° ($K^2\sim2$ a.u.). This feature has also been observed by Ref. [40] for $K^2>2.0$ a.u. and its intensity decreases for $K^2>6.6$ a.u. Reference [40] suggested that this feature was the transition $(2\sigma_g)^{-1}(1\pi_g)^3\,^3\Pi_g\leftarrow X\,^3\Sigma_g^-$. In order to elucidate the experimental observations, we calculated the excitation energy and GOS curve versus K^2 of $1\pi_g\leftarrow2\sigma_g$ based on the MSSCF method. The calculated excitation energy is 27.99 eV, which is close to the experimental one, 28.8 eV. It can be seen from the calculated GOSs in Fig. 6 that there is only one maximum in the K^2 region of 0.84–3.64 a.u., i.e., in the scattering angle region of 4°–8°, which agrees with our observation as shown in Fig. 5. Therefore based on our calculations and experiment we assign it to the transition of $(2\sigma_g)^{-1}(1\pi_g)^3\,^3\Pi_g\leftarrow X\,^3\Sigma_g^-$.

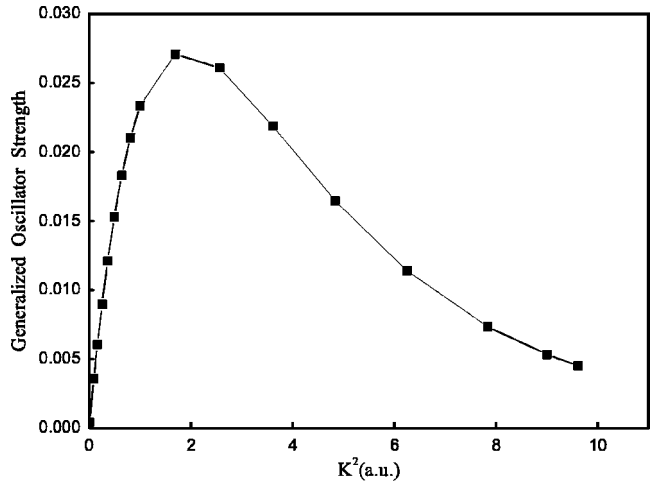

FIG. 6. The GOS of $1\pi_g\leftarrow2\sigma_g$ as a function of K^2.

IV. CONCLUSION

The electron-energy-loss spectra of O_2 have been measured at scattering angles of 0°, 2°, 4°, 6°, and 8° below 119 eV. Then the absolute OOSD spectrum and the absolute DDCS spectra have been determined. Some interesting features above the first ionization threshold become prominent as K^2 increases. Based on present experimental observations and theoretical calculations, features A_0, A_1, A_2, A_3, and A_4 are assigned to optically forbidden Rydberg series $2\sigma_u^{-1}(c\,^4\Sigma_u^-)np\sigma_u\,^3\Sigma_g^-$, $\nu'=0(n=2$–$6)$. Meanwhile, the features A_0, A_0', A_0'', and A_0''' are assigned to $\nu'=0$, 1, 2, 3 levels of $2\sigma_u^{-1}(c\,^4\Sigma_u^-)2p\sigma_u\,^3\Sigma_g^-$. The features marked A_1 and A_1' are assigned to $\nu'=0$, 1 levels of $2\sigma_u^{-1}(c\,^4\Sigma_u^-)3p\sigma_u\,^3\Sigma_g^-$. Analogously, the features marked A_2 and A_2' are assigned to $\nu'=0$, 1 levels of $2\sigma_u^{-1}(c\,^4\Sigma_u^-)4p\sigma_u\,^3\Sigma_g^-$. In addition, the present experimental quantum defects of A_0, A_1, A_2, A_3, and A_4 exhibit an oscillation, which is well explained by our calculations that a shape resonance in the $f\sigma_u$ channel occurs near threshold [3]. A feature around 28.8 eV is assigned to the transition of $(2\sigma_g)^{-1}(1\pi_g)^3\,^3\Pi_g\leftarrow X^3\Sigma_g^-$.

ACKNOWLEDGMENT

Support of this work by National Nature Science Foundation of China Grant Nos. (10004010, 10134010, 10474089) is gratefully acknowledged.

[1] M. N. Piancastelli, J. Electron Spectrosc. Relat. Phenom. **100**, 167 (1999).
[2] J. L. Dehmer and D. Dill, Phys. Rev. Lett. **35**, 213 (1975).
[3] Z. P. Zhong and J. M. Li, J. Phys. B **37**, 735 (2004).
[4] E. Shigemasa, J. Adachi, K. Soejima, N. Watanabe, A. Yagishita, and N. A. Cherepkov, Phys. Rev. Lett. **80**, 1622 (1998).
[5] N. A. Cherepkov, G. Raseev, J. Adachi, Y. Hikosaka, K. Ito, S. Motoki, M. Sano, K. Soejima, and A. Yagishita, J. Phys. B **33**, 4213 (2000).
[6] A. P. Hitchcock and C. E. Brion, J. Electron Spectrosc. Relat. Phenom. **18**, 1 (1980), and references therein.
[7] P. Lin and R. R. Lucchese, J. Chem. Phys. **116**, 8863 (2002), and references therein.
[8] J. M. Sun, Z. P. Zhong, L. F. Zhu, W. B. Li, X. J. Liu, Z. S. Yuan, and K. Z. Xu, Phys. Rev. A **70**, 012708 (2004).
[9] Z. P. Zhong, X. Y. Han, W. H. Zhang, and J. M. Li, Chin. Phys. Lett. **21**, 279 (2004).
[10] R. L. Platzman, Radiat. Res. **17**, 419 (1962).
[11] R. L. Platzman, Vortex **23**, 372 (1962).
[12] Y. Hatano, Phys. Rep. **313**, 109 (1999).
[13] S. L. Wu, Z. P. Zhong, R. F. Feng, S. L. Xing, B. X. Yang, and K. Z. Xu, Phys. Rev. A **51**, 4494 (1995).
[14] K. Z. Xu, R. F. Feng, S. L. Wu, Q. Ji, X. J. Zhang, Z. P. Zhong, and Y. Zheng, Phys. Rev. A **53**, 3081 (1996).
[15] X. J. Liu, L. F. Zhu, X. M. Jiang, Z. S. Yuan, B. Cai, X. J. Chen, and K. Z. Xu, Rev. Sci. Instrum. **72**, 3357 (2001).
[16] J. Geiger and B. Schroder, J. Chem. Phys. **49**, 740 (1968).
[17] W. F. Chan, G. Cooper, and C. E. Brion, Phys. Rev. A **44**, 186 (1991).
[18] M. Inokuti, Rev. Mod. Phys. **43**, 297 (1971).
[19] H. Bethe, Ann. Phys. **5**, 325 (1930); Z. Phys. **76**, 293 (1930).
[20] T. N. Olney, N. M. Cann, G. Cooper, and C. E. Brion, Chem. Phys. **223**, 59 (1997).
[21] J. A. Wheeler and J. A Bearden, Phys. Rev. **46**, 755 (1934).
[22] J. Dehmer, M. Inokuti, and R. P. Saxon, Phys. Rev. A **12**, 102 (1975).
[23] C. E. Brion, K. H. Tan, M. J. Van der Wiel, and Ph. E. Van der Leeuw, J. Electron Spectrosc. Relat. Phenom. **17**, 101 (1979).
[24] X. C. Pan, X. L. Liang, and J. M. Li, Acta Phys. Sin. **36**, 426 (1987) (in Chinese).
[25] L. Liu and J. M. Li, J. Phys. B **24**, 1893 (1991).
[26] K. H. Sze, C. E. Brion, X. M. Tong, and J. M. Li, Chem. Phys. **115**, 433 (1987).
[27] X. M. Tong, J. M. Li, K. H. Sze, and C. E. Brion, 14th International Conference on X-ray and Inner-shell Processes, Paris, France, 1987.
[28] X. M. Tong and J. M. Li, J. Phys. B **22**, 1531 (1989); in 16th International Conference on the Physics of Electronic and Atomic Collisions, New York, 1989.
[29] M. Dingfelder and M. Inokuti, Radiat. Environ. Biophys. **38**, 93 (1999).
[30] Cássia C. Turci, James T. Francis, Tolek Tyliszczak, G. G. de Souza, and Adam P. Hitchcock, Phys. Rev. A **52**, 4678 (1995).
[31] P. Baltzer, B. Wannberg, L. Karlsson, M. Carlsson Göthe, and M. Larsson, Phys. Rev. A **45**, 4374 (1992).
[32] N. Jonathan, A. Morris, M. Okuda, K. J. Ross, and D. J. Smith, J. Chem. Soc., Faraday Trans. 2 **70**, 1810 (1974).
[33] M. Ukai, S. Machida, K. Kameta, M. Kitajima, N. Kouchi, Y. Hatano, K. Ito, Phys. Rev. Lett. **74**, 239 (1995).
[34] P. Huber and G. Herzberg, Molecular Spectra and Molecular Structure Vol. 4 (Van Nostrand, Princeton, 1979).
[35] H. Liebel, R. Müller-Llbrecht, S. Lauer, F. Vollweiler, A. Ehresmann, and H. Schmoranzer, J. Phys. B **34**, 2581 (2001).
[36] Eisuke Nishitani, Ikuzo Tanaka, Kenichiro Tanaka, Tatsuhisa Kato, and Inosuke Koyano, J. Chem. Phys. **81**, 3429 (1984).
[37] D. Čubrić, A. A. Wills, J. Comer, and M. Ukai, J. Phys. B **26**, 3081 (1993).
[38] A. Yagishita, E. Shigemasa, and N. Kosugi, Phys. Rev. Lett. **72**, 3961 (1994), and references therein.
[39] M. A. Dillon and David Spence, J. Chem. Phys. **74**, 6070 (1981).
[40] J. S. Lee, J. Chem. Phys. **67**, 3998 (1977).